Data in brief 29 (2020) 105191

Contents lists available at ScienceDirect

Data in brief

journal homepage: www.elsevier.com/locate/dib

Data Article

# Data supporting Maastrichtian paleoclimate variables applying a multi proxy approach to a paleosol profile, Arctic Alaska

Susana Salazar-Jaramillo [a, *], Paul J. McCarthy [b], Andrés Ochoa [c], Sarah J. Fowell [d], Fred J. Longstaffe [e]

[a] Universidad Nacional de Colombia, Escuela de Geociencias, Calle 59 A No. 63 - 20 Bloque 14-215, Medellín, Colombia
[b] University of Alaska Fairbanks, Department of Geosciences, and Geophysical Institute, Fairbanks, AK, 99775-5780, USA
[c] Universidad Nacional de Colombia, Departamento de Geociencias y Medio Ambiente, Cl. 80 Nº 65 – 223, Medellín, Colombia
[d] University of Alaska Fairbanks, Department of Geosciences, Fairbanks, AK, 99775-5780, USA
[e] The University of Western Ontario, Department of Earth Sciences, London, Ontario, N6A 5B7, Canada

ARTICLE INFO

*Article history:*
Received 12 December 2019
Received in revised form 21 January 2020
Accepted 21 January 2020
Available online 25 January 2020

*Keywords:*
Maastrichtian paleo-Arctic
Paleoclimate
Meteoric water composition
Silicate weathering

ABSTRACT

We provide the dataset of climate variables related to the research article "Paleoclimate reconstruction of the Prince Creek Formation, Arctic Alaska, during Maastrichtian global warming" [1]. The dataset includes mean annual precipitation (MAP) values determined using two independent proxies, estimates of the oxygen isotope composition of meteoric water ($\delta^{18}O_w$) obtained from smectites and a comparison with previously published siderite data. We also provide the data used to calculate the total flux of $CO_2$ required for the weathering of silicates. This dataset is an example of a multi proxy approach that could add further insight for researchers in the selection of suitable proxies for paleoclimatic interpretations.



DOI of original article: https://doi.org/10.1016/j.palaeo.2019.109265.
* Corresponding author.
*E-mail address:* ssalazarj@unal.edu.co (S. Salazar-Jaramillo).

https://doi.org/10.1016/j.dib.2020.105191

Specifications Table

| | |
|---|---|
| Subject | Earth and Planetary Sciences: Earth-Surface Processes |
| Specific subject area | Paleoclimatology of a Maastrichtian paleosol profile in the paleo-Arctic using geochemical proxies. |
| Type of data | Tables<br>Figures<br>Raw data |
| How data were acquired | *XRF:* PANalytical Axios wavelength-dispersive X-ray fluorescence spectrometer (WD-XRF); *mass spectrometry* for $\delta^{13}C$: EA-IRMS (Elemental Analysis - Isotope Ratio Mass Spectrometry), Elemental Analyzer (ECS 4010); *mass spectrometry* for $\delta^{18}O$: Micromass Optima dual-inlet, IRMS; *software*: IDL. Details on analytical techniques in Ref. [1] and the section Experimental Design, Materials, and Methods. |
| Data format | Raw and analized data are provided in Tables 1–5 and in excel files as supplementary material. |
| Parameters for data collection | Field collection of bulk paleosol samples from a paleosol profile near the Kikak-Tegoseak dinosaur bonebed from bluffs along the Colville River, Alaska. |
| Description of data collection | Data collected included pedologic and sedimentologic macrostructures and microstructures, color, major oxide geochemistry, and total organic carbon (TOC) of paleosol samples. Details of the profile description are given in Ref. [2]. For the detailed geochemical analysis, one paleosol profile and two bentonite layers (NKT) were chosen. Samples were carefully taken every 20 cm after soil profile description according to Ref. [2]. Samples were air-dried and analysed according to the analytical techniques we describe in the section Experimental Design, Materials, and Methods. |
| Data source location | *Colville River, Alaska, U.S.,* paleosol profile: *N 69° 45.068′; W 151° 30.873′*; bentonites *N 69° 38.651′; W 151° 50.565′* and *N 69° 41.012′; W 151° 30.481′* |
| Data accessibility | All data are available within this article. |
| Related research article | Associated Paper: Salazar-Jaramillo S., McCarthy P.J., Ochoa A., Fowell, S.J., Longstaffe, F.J. Paleoclimate reconstruction of the Prince Creek Formation, Arctic Alaska, during Maastrichtian global warming. Palaeogeogr. Palaeoclimatol. Palaeoecol. 2019; 532 (July):109265. https://doi.org/10.1016/j.palaeo.2019.109265. |

**Value of the Data**

- The climatic variables provide information regarding the Cretaceous paleo-Arctic that can be compared with previously published independent qualitative and quantitative data.
- The data allow assessment of Cretaceous General Circulation Model (GCM) simulations through data-model comparisons.
- The carbon isotopic composition ($\delta^{13}C$), obtained in paleosols from pollen and bulk organic matter, is valuable as a reference to refine proxies used in the identification of carbon cycle perturbations.
- The oxygen isotopic composition of meteoric water ($\delta^{18}O_w$) derived from smectite provides information as a paleohydrologic indicator, extending the sampling of high latitude continental deposits to pedogenic clays.
- The total flux of $CO_2$ required for silicate weathering is useful to understand the $CO_2$ sinks in the geological carbon cycle in Maastrichtian arctic paleosols.

## 1. Data description

In this article, we report raw data of carbon and nitrogen isotopes (from pollen and bulk organic matter) in Table 1. Data of major elements from a Maastrichtian paleosol profile ($n = 7$) are reported in Table 2. These data are reported as raw, and as molar proportions, for the A-C*N-K diagram plotted in Ref. [1], using $Al_2O_3$, $CaO^* + Na_2O$, $K_2O$, according to Ref. [3]. Both, raw and analysed oxygen isotope data from the total clay-size fraction for the NKT paleosol ($n = 7$) and from the KKT and PFDV bentonites ($n = 2$) are reported in Tables 3 and 4, respectively. Table 4 and Fig. 1 also report the calculated $\delta^{18}O_w$ (‰. VSMOW) of meteoric water using the equation of Sheppard and Gilg [4], and compare the data with $\delta^{18}O_w$ from siderite [5]. Fig. 2 is a plot of mean annual precipitation using three equations

**Table 1**
Nitrogen (N), organic carbon (C), $\delta^{15}N$, $\delta^{13}C$ and C/N ratio values of bulk samples (NKT) and palynologic separates (NKT-P).

| Sample Name | Conc N | Conc C | $\delta^{15}N$ At−air | $\delta^{13}C$ VPDB | C/N |
|---|---|---|---|---|---|
| | (%) | (%) | (‰) | (‰) | |
| NKT34 | 0.12 | 1.21 | +3.03 | −27.45 | 9.80 |
| NKT36 | | | | | |
| NKT38 | 0.08 | 0.26 | +2.58 | −25.23 | 3.28 |
| NKT40 | 0.07 | 0.31 | +2.71 | −25.19 | 4.17 |
| NKT42 | | | | | |
| NKT44 | 0.14 | 0.71 | +2.72 | −25.95 | 4.98 |
| NKT46 | 0.10 | 0.54 | +2.30 | −25.03 | 5.53 |
| Average | 0.10 | 0.61 | +2.67 | −25.77 | 5.55 |
| Stand.dev. | 0.03 | 0.38 | 0.26 | 1.00 | 2.52 |
| NKT34−P | 1.49 | 47.28 | +3.02 | −28.12 | 31.63 |
| NKT36−P | 1.38 | 55.82 | +2.43 | −25.61 | 40.41 |
| NKT38−P | 1.41 | 59.03 | +2.48 | −25.24 | 41.95 |
| NKT40−P | 0.95 | 33.99 | +2.76 | −25.44 | 35.88 |
| NKT42−P | 0.64 | 19.65 | +4.83 | −27.48 | 30.48 |
| NKT44−P | 1.20 | 47.83 | +3.51 | −27.39 | 39.80 |
| NKT46−P | 1.43 | 50.38 | +2.27 | −25.73 | 35.18 |
| Average | 1.22 | 44.85 | +3.04 | −26.43 | 36.48 |
| Stand.dev. | 0.31 | 13.66 | 0.89 | 1.19 | 4.43 |

(and several $\delta^{13}C$ atmospheric scenarios, [1]) that estimate MAP from $\delta^{13}C$ in pollen [6,7]. Table 5 and Fig. 3 show analysed data for mass balance calculations [8], and Fig. 4 indicates mass-balance calculations that relate elemental weathering to atmospheric $CO_2$ levels (given in [mol/cm$^2$]) [9,10].

**Table 2**
Geochemical XRF raw data (in weight percent) and calculated CIA-K values [11] for the NKT paleosol.

| sample | NKT 34 | NKT 36 | NKT 38 | NKT 40 | NKT 42 | NKT 44 | NKT 46 |
|---|---|---|---|---|---|---|---|
| depth, m | 12.1 | 12.5 | 12.8 | 13.2 | 13.6 | 13.9 | 14.1 |
| $SiO_2$ | 69.240 | 70.170 | 71.090 | 71.600 | 65.610 | 67.960 | 68.520 |
| $TiO_2$ | 0.930 | 0.940 | 0.910 | 0.860 | 0.790 | 0.950 | 0.930 |
| $Al_2O_3$ | 17.710 | 17.070 | 16.900 | 15.990 | 16.930 | 18.900 | 17.590 |
| $Fe_2O_3$ | 4.680 | 5.190 | 4.040 | 4.920 | 14.300 | 4.660 | 5.590 |
| MnO | 0.020 | 0.060 | 0.020 | 0.040 | 0.270 | 0.030 | 0.130 |
| MgO | 1.820 | 1.760 | 1.740 | 1.630 | 1.700 | 1.880 | 2.000 |
| CaO | 0.160 | 0.170 | 0.170 | 0.170 | 0.840 | 0.150 | 0.320 |
| $Na_2O$ | 1.510 | 1.480 | 1.560 | 1.580 | 1.610 | 1.430 | 1.380 |
| $K_2O$ | 3.000 | 2.930 | 2.760 | 2.470 | 2.010 | 3.110 | 3.110 |
| $P_2O_5$ | 0.040 | 0.040 | 0.050 | 0.040 | 0.080 | 0.050 | 0.120 |
| LOI | 0.811 | 0.334 | 0.241 | 0.214 | 0.253 | 0.913 | 0.550 |
| Sum | 99.921 | 100.144 | 99.481 | 99.514 | 104.393 | 100.033 | 100.240 |
| Molar proportions [3] | | | | | | | |
| CaO* (mol) | 0.002 | 0.002 | 0.002 | 0.002 | 0.013 | 0.002 | 0.003 |
| $Al_2O_3$ (mol) | 0.174 | 0.167 | 0.166 | 0.157 | 0.166 | 0.185 | 0.173 |
| $Na_2O$ (mol) | 0.024 | 0.024 | 0.025 | 0.025 | 0.026 | 0.023 | 0.022 |
| $K_2O$ (mol) | 0.032 | 0.031 | 0.029 | 0.026 | 0.021 | 0.033 | 0.033 |
| A-C*N-K | | | | | | | |
| A | 0.749 | 0.746 | 0.746 | 0.745 | 0.733 | 0.763 | 0.748 |
| C*N | 0.113 | 0.116 | 0.122 | 0.131 | 0.173 | 0.101 | 0.109 |
| K | 0.137 | 0.139 | 0.132 | 0.124 | 0.094 | 0.136 | 0.143 |
| Sum | 1.000 | 1.000 | 1.000 | 1.000 | 1.000 | 1.000 | 1.000 |
| CIA-K | 86.860 | 86.570 | 85.980 | 85.042 | 80.949 | 88.295 | 87.275 |

**Table 3**
Calculated $\delta^{18}O$ (‰ VSMOW) of meteoric water from the total clay-size fraction for the NKT paleosol and the KKT and PFDV bentonites. The last column is the calculated $\delta^{18}O$ of meteoric water using temperatures (−2 °C minimum, 6.3 °C average, and 14.5 °C maximum) determined from CLAMP analysis of paleobotanical specimens [14].

| Sample | T (C) | T (K) | $2.55 \times (10^6/T^2) - 4.05$ [4] | $\delta^{18}O$ Smectite (‰) | $\delta^{18}O$ of Meteoric water |
|---|---|---|---|---|---|
| NKT-34 | −2.00 | 271.15 | 30.63 | 12.62 | −18.01 |
| | 6.30 | 279.45 | 28.60 | 12.62 | −15.98 |
| | 14.50 | 287.65 | 26.77 | 12.62 | −14.15 |
| NKT-36 | −2.00 | 271.15 | 30.63 | 11.86 | −18.77 |
| | 6.30 | 279.45 | 28.60 | 11.86 | −16.74 |
| | 14.50 | 287.65 | 26.77 | 11.86 | −14.91 |
| NKT-38 | −2.00 | 271.15 | 30.63 | 11.65 | −18.98 |
| | 6.30 | 279.45 | 28.60 | 11.65 | −16.95 |
| 14.50 | 287.65 | 26.77 | 11.65 | −15.12 | |
| NKT-40 | −2.00 | 271.15 | 30.63 | 11.48 | −19.15 |
| | 6.30 | 279.45 | 28.60 | 11.48 | −17.12 |
| | 14.50 | 287.65 | 26.77 | 11.48 | −15.29 |
| NKT-42 | −2.00 | 271.15 | 30.63 | 12.36 | −18.27 |
| | 6.30 | 279.45 | 28.60 | 12.36 | −16.24 |
| | 14.50 | 287.65 | 26.77 | 12.36 | −14.41 |
| NKT-44 | −2.00 | 271.15 | 30.63 | 12.28 | −18.35 |
| | 6.30 | 279.45 | 28.60 | 12.28 | −16.32 |
| | 14.50 | 287.65 | 26.77 | 12.28 | −14.49 |
| NKT-46 | −2.00 | 271.15 | 30.63 | 12.17 | −18.46 |
| | 6.30 | 279.45 | 28.60 | 12.17 | −16.43 |
| | 14.50 | 287.65 | 26.77 | 12.17 | −14.60 |
| D6KKT-20.5 | −2.00 | 271.15 | 30.63 | 4.96 | −25.67 |
| | 6.30 | 279.45 | 28.60 | 4.96 | −23.64 |
| | 14.50 | 287.65 | 26.77 | 4.96 | −21.81 |
| PFDV-17-5.7 | −2.00 | 271.15 | 30.63 | 5.03 | −25.60 |
| | 6.30 | 279.45 | 28.60 | 5.03 | −23.57 |
| | 14.50 | 287.65 | 26.77 | 5.03 | −21.74 |

## 2. Experimental design, materials, and methods

Seventy-five sections of the Prince Creek Formation were measured and described for grain size and sedimentary structures [2]. The NKT site (*N 69° 45.068′; W 151° 30.873′*) was selected for paleosol study based on accessibility of outcrop and abundance of paleopedological features. Macroscopic features including color, grain size, ped structure, mottles, nodules, root traces, flora and fauna were described in detail in Ref. [2]. Bulk samples were collected at 15–30 cm intervals and all samples were air-dried. Total organic carbon (TOC) was determined by Weatherford Laboratories, Shenandoah, Texas. Samples were pulverized, sieved, and reacted with concentrated HCl to dissolve carbonates. Samples were dried and combusted in a LECO model C230 combustion furnace, and $CO_2$ generated by the combustion of organic matter was quantified using an infrared detector to determine TOC. Detailed description of the sampling method is given in Ref. [2], and a detailed description of geochemical processing and analytical methods is given in Ref. [1].

### 2.1. $\delta^{13}C$ analyses of pollen grains

Sediment samples were mechanically disaggregated and treated with 10% HCl to remove carbonate, and with 49% HF to remove silicates. Samples were washed with de-ionized water several times to neutralize the acid. The final wash was through a 250 μm sieve. Sodium polytungstate was used as a heavy liquid to separate the organic fraction from remaining minerals. After freeze-drying, pollen samples were weighed for $\delta^{13}C$ analyses. The C and N analyses (Table 1) were conducted at the Alaska Stable Isotope Facility (ASIF), University of Alaska Fairbanks. $\delta^{13}C$ was measured using EA-IRMS. This method utilizes a Costech Elemental Analyzer (ESC 4010), and Thermo Conflo III interface with a DeltaV Mass Spectrometer [1].

**Table 4**
Calculated $\delta^{18}O$ (‰ VSMOW) of meteoric water derived from the Prince Creek Formation at several temperatures. Data from smectites (bentonites and total clay) are estimated based on the fractionation equation of [4]. In order to compare with published values, the siderite data are taken from Ref. [5], which uses the fractionation equation of [12].

| T (C) | T (K) | 1000 Ln $\alpha_{x\text{-}w}$ | | $\delta^{18}O$ of Meteoric water using the following: $\delta^{18}O$ Sid and $\delta^{18}O$ Sm values (SMOW) | | | | | |
|---|---|---|---|---|---|---|---|---|---|
| | | $3.13 \times (10^6/T^2) - 3.5$ | $2.55 \times (10^6/T^2) - 4.05$ | $\delta^{18}O$ Sid = +14.21‰ | $\delta^{18}O$ Sid = +15.60‰ | $\delta^{18}O$ Sm = +4.96‰ | $\delta^{18}O$ Sm = +5.03‰ | $\delta^{18}O$ Sm = +11.48‰ | $\delta^{18}O$ Sm = +12.62‰ |
| | | [12] | [4] | [5] | | This work | | | |
| −14.50 | 258.65 | 43.29 | 34.07 | −29.08 | −27.69 | −29.11 | −29.04 | −22.59 | −21.45 |
| −10.00 | 263.15 | 41.70 | 32.77 | −27.49 | −26.10 | −27.81 | −27.74 | −21.29 | −20.15 |
| −5.00 | 268.15 | 40.03 | 31.41 | −25.82 | −24.43 | −26.45 | −26.38 | −19.93 | −18.79 |
| −2.00 | 271.15 | 39.07 | 30.63 | −24.86 | −23.47 | −25.67 | −25.60 | −19.15 | −18.01 |
| 0.00 | 273.15 | 38.45 | 30.13 | −24.24 | −22.85 | −25.17 | −25.10 | −18.65 | −17.51 |
| 5.00 | 278.15 | 36.96 | 28.91 | −22.75 | −21.36 | −23.95 | −23.88 | −17.43 | −16.29 |
| 6.30 | 279.45 | 36.58 | 28.60 | −22.37 | −20.98 | −23.64 | −23.57 | −17.12 | −15.98 |
| 10.00 | 283.15 | 35.54 | 27.76 | −21.33 | −19.94 | −22.80 | −22.73 | −16.28 | −15.14 |
| 14.50 | 287.65 | 34.33 | 26.77 | −20.12 | −18.73 | −21.81 | −21.74 | −15.29 | −14.15 |
| 15.00 | 288.15 | 34.20 | 26.66 | −19.99 | −18.60 | −21.70 | −21.63 | −15.18 | −14.04 |
| 20.00 | 293.15 | 32.92 | 25.62 | −18.71 | −17.32 | −20.66 | −20.59 | −14.14 | −13.00 |
| 25.00 | 298.15 | 31.71 | 24.64 | −17.50 | −16.11 | −19.68 | −19.61 | −13.16 | −12.02 |
| 30.00 | 303.15 | 30.56 | 23.70 | −16.35 | −14.96 | −18.74 | −18.67 | −12.22 | −11.08 |
| 35.00 | 308.15 | 29.46 | 22.80 | −15.25 | −13.86 | −17.84 | −17.77 | −11.32 | −10.18 |
| 40.00 | 313.15 | 28.42 | 21.95 | −14.21 | −12.82 | −16.99 | −16.92 | −10.47 | −9.33 |
| 45.00 | 318.15 | 27.42 | 21.14 | −13.21 | −11.82 | −16.18 | −16.11 | −9.66 | −8.52 |
| 50.00 | 323.15 | 26.47 | 20.37 | −12.26 | −10.87 | −15.41 | −15.34 | −8.89 | −7.75 |
| 55.00 | 328.15 | 25.57 | 19.63 | −11.36 | −9.97 | −14.67 | −14.60 | −8.15 | −7.01 |
| 60.00 | 333.15 | 24.70 | 18.93 | −10.49 | −9.10 | −13.97 | −13.90 | −7.45 | −6.31 |

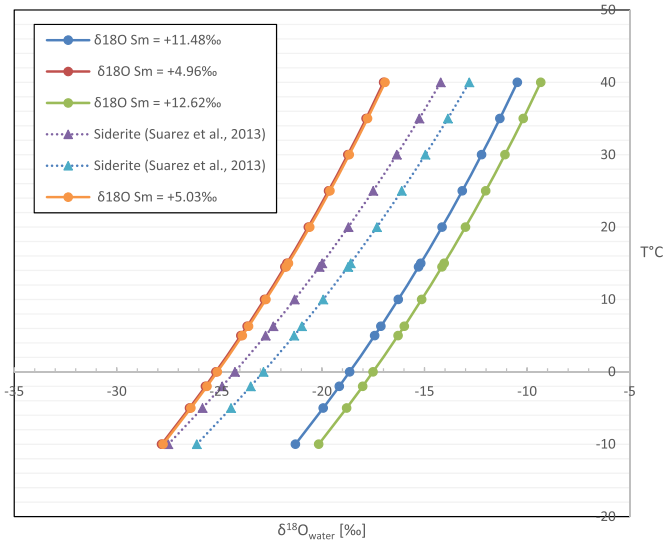


**Fig. 1.** Solid lines show the isotopic composition of meteoric water derived from smectites based on the isotopic fractionation between smectite and meteoric water [4] using the maximum and minimum $\delta^{18}O$ of bulk clay and bentonites. The dashed lines correspond to the meteoric water isotopic composition calculated using pedogenic siderite [5].

### 2.2. XRF analyses

Samples were prepared by powdering using hardened steel vials from SPEX CertiPrep Group, and pressed into 35 mm diameter pellets using a polyvinyl alcohol binder. Abundances (in wt. %) of the light major oxides ($SiO_2$, $Al_2O_3$, $Fe_3O_3$, $Na_2O$, MgO, $P_2O_5$, $K_2O$, CaO, MnO and $TiO_2$) (Table 2) were measured from bulk samples using a PANalytical Axios wavelength-dispersive X-ray fluorescence spectrometer (WD-XRF) at the University of Alaska Fairbanks Advanced Instrumentation Laboratory (AIL) [1]. The chemical index of alteration minus potassium (CIA-K) was calculated according to Ref. [11] (Table 2).

### 2.3. $\delta^{18}O$ analyses of clay samples

The total clay (<2 μm fraction) was separated using the hydrometer method. After mixing the slurry in a settling column, we used a settling time of 23 h 16 min for a 30 cm settling column at T = 20 °C room temperature. We used a pipette to siphon the supernatant into the centrifuge tubes. Then the <0.2 μm clay fraction was separated by centrifuging for approximately 6 minutes at 11,000 rpm, where the time and speed was calculated with Centriset, a USGS program, which computes settling velocity based on Stokes Law for gravitational procedures. All samples (the <2 μm and <0.2 μm fractions) were freeze-dried for stable isotope analysis. $\delta^{18}O$ values (Table 3) were measured using a Micromass Optima dual-inlet, IRMS in the Laboratory for Stable Isotope Science at the University of Western Ontario, London, Canada [1].

### 2.4. Meteoric water composition data

We determined meteoric water composition (Table 3; Fig. 1) using the relationship that describes the oxygen isotope fractionation between smectite and water [4]. Table 4 and Fig. 1, show the relationship between meteoric water composition and temperature for maximum and minimum smectite $\delta^{18}O$ values and compare these data with previous studies of meteoric water composition calculated from siderite [5] using the equation of [12].

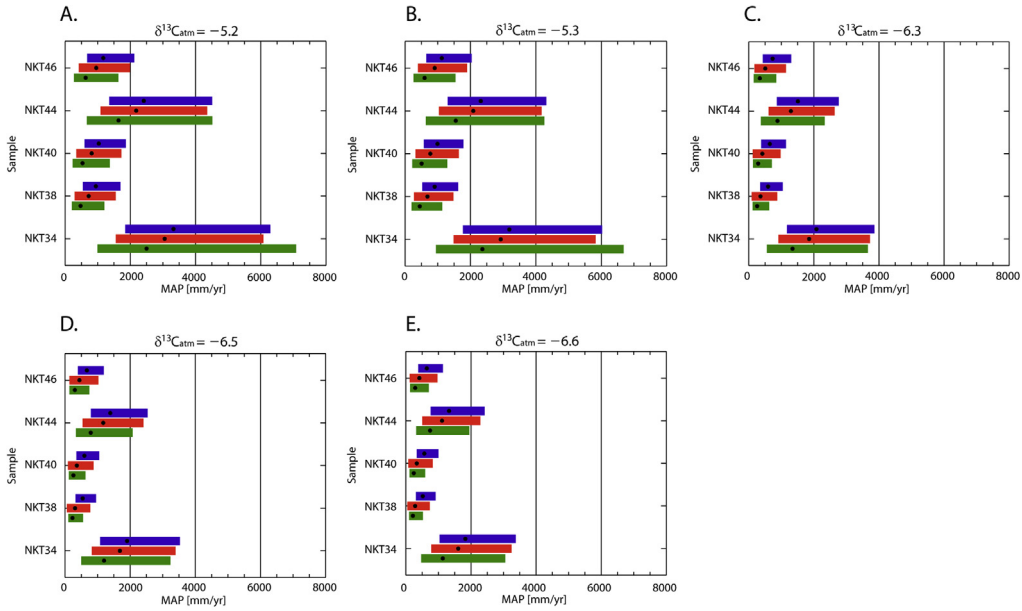


Diefendorf: $\Delta_{leaf}$=(5.54±0.22)*log$_{10}$(MAP)+(4.07±0.70)

The maximum and minimum limits are:

$$MAP_{Min} = 10^{\frac{\Delta_{leaf} - (4.07 + 0.70)}{5.54 + 0.22}}$$

$$MAP_{Max} = 10^{\frac{\Delta_{leaf} - (4.07 - 0.70)}{5.54 - 0.22}}$$

Code nomenclature:

MAP min= 10^ ((Dleaf-(4.07+ 0.70))/(5.54+ 0.22))

MAP max= 10^ ((Dleaf-(4.07-0.70))/(5.54-0.22))

Diefendorf: $\Delta_{leaf}$=(4.20±0.26)*log$_{10}$(MAP)−(0.06±0.01)*sqrt(z)+(9.31±0.90)

The maximum and minimum limits are:

$$MAP_{Min} = 10^{\frac{\Delta_{leaf} + (0.06 - 0.01) \cdot \sqrt{z} - (9.31+0.90)}{4.20 + 0.26}}$$

$$MAP_{Max} = 10^{\frac{\Delta_{leaf} + (0.06 + 0.01) \cdot \sqrt{z} - (9.31 - 0.90)}{4.20 - 0.26}}$$

Code nomenclature:

MAPmax=10^ ((Dleaf+(0.06+0.01)*sqrt(Altitude)-(9.31-0.90))/(4.20-0.26))

MAPmin=10^ ((Dleaf+(0.06-0.01)*sqrt(Altitude)-(9.31+0.90))/(4.20+0.26))

Kohn: $\Delta_{leaf}$=(2.01±0.73)−(0.00±0.00)*Altitude+(5.88±0.24)*log$_{10}$(MAP+300)+(0.01±0.00)*Abs(latitude)

The maximum and minimum limits are:

$$MAP_{Min} = 10^{\frac{(2.01 + 0.73) + (0.00 - 0.00) \cdot z - (0.01 + 0.00) \cdot |\varphi|}{5.88 + 0.24}} - 300$$

$$MAP_{Max} = 10^{\frac{(2.01 - 0.73) + (0.00 + 0.00) \cdot z - (0.01 - 0.00) \cdot |\varphi|}{5.88 - 0.24}} - 300$$

Code nomenclature:

MAPmin=10^((Dleaf-(2.01+0.73)+(0.00-0.00)*Altitude-(0.01+0.00)*abs(Latitude))/(5.88+0.24))-300.

MAPmax=10^((Dleaf-(2.01-0.73)+(0.00+0.00)*Altitude-(0.01-0.00)*abs(Latitude))/(5.88-0.24))-300.

**Fig. 2.** MAP variability in the Prince Creek Formation using $\delta^{13}C_{atm}$ from several authors (Table 3 in Ref. [1]) in the [6,7] equations. A-E) Mean annual precipitation (MAP) using minimum and maximum values as indicated in the equations, where the black dot is the mean value. At the top of each plot are the corresponding $\delta^{13}C_{atm}$ values used. The colors are related to the equation being used.

**Table 5**
Depth, after applying a paleosol compaction equation [15], bulk density, and strain (ε) and elemental mass transport (τ) for mass balance calculations [8].

| dZ (m)] | Depth (m) | Sample | Bulk density | Strain | $SiO_2$ | $Al_2O_3$ | $Fe_2O_3$ | $Na_2O$ | MgO | $P_2O_5$ | $K_2O$ | CaO | MnO |
|---|---|---|---|---|---|---|---|---|---|---|---|---|---|
| 0.20 | 12.10 | NKT 34 | 2.00 | 0.00 | 0.00 | 0.00 | 0.00 | 0.00 | 0.00 | 0.00 | 0.00 | 0.00 | 0.00 |
| 0.35 | 12.50 | NKT 36 | 1.96 | 0.01 | 0.00 | −0.05 | 0.10 | −0.03 | −0.04 | −0.01 | −0.03 | 0.05 | 1.97 |
| 0.35 | 12.80 | NKT 38 | 2.15 | −0.05 | 0.05 | −0.02 | −0.12 | 0.06 | −0.02 | 0.28 | −0.06 | 0.09 | 0.02 |
| 0.40 | 13.20 | NKT 40 | 1.79 | 0.21 | 0.12 | −0.02 | 0.14 | 0.13 | −0.03 | 0.08 | −0.11 | 0.15 | 1.16 |
| 0.35 | 13.60 | NKT 42 | 2.23 | 0.06 | 0.12 | 0.13 | 2.60 | 0.26 | 0.10 | 1.35 | −0.21 | 5.18 | 14.89 |
| 0.25 | 13.90 | NKT 44 | 1.96 | 0.00 | −0.04 | 0.04 | −0.03 | −0.07 | 0.01 | 0.22 | 0.01 | −0.08 | 0.47 |
| 0.10 | 14.10 | NKT 46 | 2.04 | −0.02 | −0.01 | −0.01 | 0.19 | −0.09 | 0.10 | 2.00 | 0.04 | 1.00 | 5.50 |

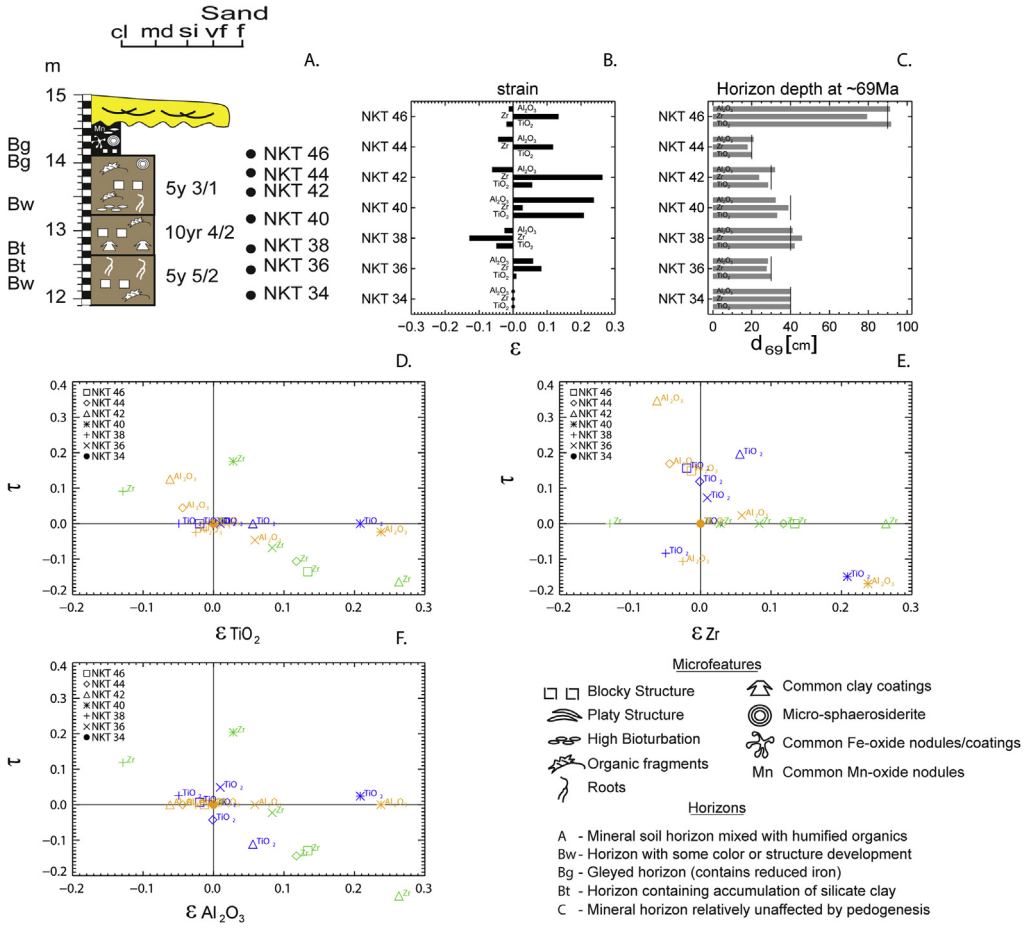


**Fig. 3.** A) NKT paleosol horizons and depth. B) Strain (ε). Volume change during weathering [8] calculated for the NKT paleosol. C) Thickness after applying a paleosol compaction equation at ~69 Ma [15]. (D–E) Mass balance cross-plots of strain (ε) vs. elemental mass transport (τ) for the NKT paleosol using $TiO_2$ (blue), Zr (green), and $Al_2O_3$ (yellow). The calculations assume immobility of D) $TiO_2$, E) Zr, and F) $Al_2O_3$.

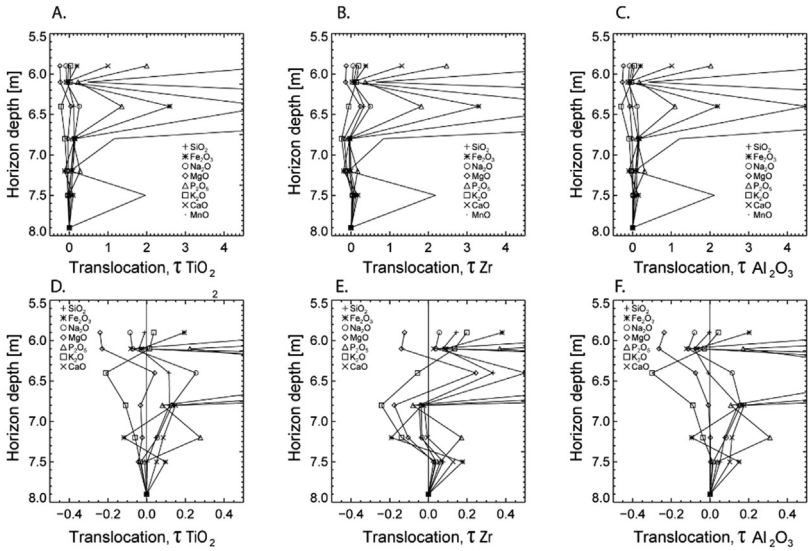


$CO_2$ moles removed:
$CO_2$ removed by $SiO_2$ [mol/cm$^2$]: −0.0801337
$CO_2$ removed by $Fe_2O_3$ [mol/cm$^2$]: −0.00640170
$CO_2$ removed by $Na_2O$ [mol/cm$^2$]: −0.0100020
$CO_2$ removed by MgO [mol/cm$^2$]: −0.0543834
$CO_2$ removed by $P_2O_5$ [mol/cm$^2$]:−3.56341e−006
$CO_2$ removed by $K_2O$ [mol/cm$^2$]: −0.0167529
$CO_2$ removed by CaO [mol/cm$^2$]: −0.000187912

Total $CO_2$ removed based on $TiO_2$ [mol/cm$^2$]: −0.167865
Total $CO_2$ removed by Na, Mg, K and Ca [mol/cm$^2$]: −0.0813262

$CO_2$ moles removed:
$CO_2$ removed by $SiO_2$ [mol/cm$^2$]: −0.168346
$CO_2$ removed by $Fe_2O_3$ [mol/cm$^2$]: −0.0117999
$CO_2$ removed by $Na_2O$ [mol/cm$^2$]: −0.00286296
$CO_2$ removed by MgO [mol/cm$^2$]: −0.0432063
$CO_2$ removed by $P_2O_5$ [mol/cm$^2$]:−3.50902e−005
$CO_2$ removed by $K_2O$ [mol/cm$^2$]: −0.0218210
$CO_2$ removed by CaO [mol/cm$^2$]: −0.000125113

Total $CO_2$ removed based on Zr [mol/cm$^2$]: −0.248229
Total $CO_2$ removed by Na, Mg, K and Ca [mol/cm$^2$]: −0.0680154

$CO_2$ moles removed:
$CO_2$ removed by $SiO_2$ [mol/cm$^2$]: −0.105666
$CO_2$ removed by $Fe_2O_3$ [mol/cm$^2$]: −0.00623000
$CO_2$ removed by $Na_2O$ [mol/cm$^2$]: −0.00939120
$CO_2$ removed by MgO [mol/cm$^2$]: −0.0537094
No $P_2O_5$ loss $Al_2O_3$.
$CO_2$ removed by $K_2O$ [mol/cm$^2$]: −0.0184526
$CO_2$ removed by CaO [mol/cm$^2$]: −0.000290113

Total $CO_2$ removed based on $Al_2O_3$ [mol/cm$^2$]: −0.193739
Total $CO_2$ removed by Na, Mg, K and Ca [mol/cm$^2$]: −0.0818433

**Fig. 4.** Elemental translocation (transport) assuming immobile A) $TiO_2$, B) Zr, and C) $Al_2O_3$. Images (D–F) are the same translocations without the element Mn. At the bottom of the figure are mass-balance calculations that relate elemental weathering to atmospheric $CO_2$ levels (given in [mol/cm$^2$]) [9,10].

### 2.5. Mean annual precipitation (MAP) data

We calculated MAP values (Fig. 2) following equations [6,7], and [13] (details in Ref. [1]).

### 2.6. Mass balance and total flux of $CO_2$ data

Mass balance calculations [8] are shown in Table 5 and Fig. 3. Fig. 4 indicates the total $CO_2$ flux calculated from mass balance [9,10] that was used to determine silicate weathering (the moles of $CO_2$ that react as carbonic acid to release K, Ca, Mg, and Na base cations).

## Acknowledgments

Financial support for the collection of paleosol and bentonite samples used in this research was provided by the National Science Foundation Office of Polar Programs (OPP 0424594 and OPP 0425636). Additional support for subsequent laboratory analyses was provided by the University of Alaska Museum of the North, the Clay Minerals Society, and the Natural Sciences and Engineering Research Council of Canada. The authors wish to thank the International Association of Sedimentologists (IAS) and Colciencias Colombia for economic support. The authors also thank Gordon Medaris for his assistance with data analyses for CIA. This is Laboratory for Stable Isotope Science Contribution #367.

## Conflict of Interest

The authors declare that they have no known competing financial interests or personal relationships that could have appeared to influence the work reported in this paper.

## Appendix A. Supplementary data

Supplementary data to this article can be found online at https://doi.org/10.1016/j.dib.2020.105191.

## References

[1] S. Salazar-Jaramillo, P.J. McCarthy, A. Ochoa, S.J. Fowell, F.J. Longstaffe, Paleoclimate reconstruction of the Prince Creek Formation, Arctic Alaska, during Maastrichtian global warming, Palaeogeogr. Palaeoclimatol. Palaeoecol. 532 (July) (2019) 109265, https://doi.org/10.1016/j.palaeo.2019.109265.

[2] P.P. Flaig, P.J. Mccarthy, A.R. Fiorillo, Anatomy, evolution and Paleoenvironmental interpretation of an Ancient Arctic Coastal plain: integrated Paleopedology and Palynology from the upper Cretaceous (Maastrichtian) Prince Creek formation, North Slope, Alaska, in: S.G. Driese, L.C. Nordt (Eds.) vol. 104, SEPM Spec Publ, 2013, pp. 179–230.

[3] C.M. Fedo, H.W. Nesbitt, G.M. Young, Unravelling the effects of potassium metasomatism in sedimentary rocks and paleosols, with implications for paleoweathering conditions and provenance, Geology 23 (10) (1995) 921–924, https://doi.org/10.1130/0091-7613(1995)023<0921:UTEOPM>2.3.CO.

[4] S.M.F. Sheppard, H.A. Gilg, Stable Isotope geochemistry of clay minerals, Clay Miner. 31 (1996) 1–24, https://doi.org/10.1180/claymin.1996.031.1.01.

[5] M.B. Suarez, G.A. Ludvigson, L.A. González, A.H. Al-Suwaidi, H.-L. You, Stable isotope chemostratigraphy in lacustrine strata of the Xiagou formation, Gansu province, NW China, in: A.-V. Bojar, M.C. Melinte-Dobrinescu, J. Smit (Eds.), Isotopic Studies in Cretaceous Research, vol. 382, The Geological Society of London, London, 2013, pp. 143–155, https://doi.org/10.1144/SP382.1.

[6] M.J. Kohn, Carbon isotope compositions of terrestrial C3 plants as indicators of (paleo)ecology and (paleo)climate, Proc. Natl. Acad. Sci. U. S. A. 107 (46) (2010) 19691–19695, https://doi.org/10.1073/pnas.1004933107.

[7] A.F. Diefendorf, K.E. Mueller, S.L. Wing, P.L. Koch, K.H. Freeman, Global patterns in leaf 13C discrimination and implications for studies of past and future climate, Proc. Natl. Acad. Sci. U. S. A. 107 (13) (2010) 5738–5743, https://doi.org/10.1073/pnas.0910513107.

[8] G.H. Brimhall, J.L. Christopher, C. Ford, J. Bratt, G. Taylor, O. Warin, Quantitative geochemical approach to pedogenesis: importance of parent material reduction, volumetric expansion, and eolian influx in lateritization, Geoderma 51 (1–4) (1991) 51–91, https://doi.org/10.1016/0016-7061(91)90066-3.

[9] H.D. Holland, E.A. Zbinden, Paleosols and the Evolution of the Atmosphere Part I. Lerman A, in: M. Meybeck (Ed.) 251, Phys Chem Weather Geochemical Cycles NATO ASI Ser, 1988, pp. 61–82, https://doi.org/10.1007/978-94-009-3071-1_12.

[10] N.D. Sheldon, N.J. Tabor, Quantitative paleoenvironmental and paleoclimatic reconstruction using paleosols, Earth Sci. Rev. 95 (1–2) (2009) 1–52, https://doi.org/10.1016/j.earscirev.2009.03.004.

[11] J.B. Maynard, Chemistry of modern soils as a guide to interpreting precambrian paleosols, J. Geol. 100 (3) (1992) 279–289, https://doi.org/10.1086/629632.

[12] W.W. Carothers, L.H. Adami, R.J. Rosenbauer, Experimental oxygen isotope fractionation between siderite-water and phosphoric acid liberated CO2-siderite, Geochim. Cosmochim. Acta 52 (10) (1988) 2445–2450, https://doi.org/10.1016/0016-7037(88)90302-X.

[13] N.D. Sheldon, G.J. Retallack, S. Tanaka, Geochemical Climofunctions from North American soils and application to paleosols across the Eocene-Oligocene Boundary in Oregon, J. Geol. 110 (2002) 687–696, https://doi.org/10.1086/342865.

[14] R.A. Spicer, A.B. Herman, The late Cretaceous environment of the arctic: a quantitative reassessment based on plant fossils, Palaeogeogr. Palaeoclimatol. Palaeoecol. 295 (3–4) (2010) 423–442, https://doi.org/10.1016/j.palaeo.2010.02.025.

[15] N.D. Sheldon, G.J. Retallack, Equation for compaction of paleosols due to burial, Geology 29 (3) (2001) 247–250, https://doi.org/10.1130/0091-7613(2001)029<0247:EFCOPD>2.0.CO;2.